

PAPER

## Neglected culprit of nonlinear discharge characteristics in SF<sub>6</sub>: shielding effect induced by positive glow corona discharge

To cite this article: Zhicheng Wu *et al* 2019 *Plasma Sources Sci. Technol.* **28** 085018

View the [article online](#) for updates and enhancements.









**IOP | ebooks™**

Bringing you innovative digital publishing with leading voices to create your essential collection of books in STEM research.

Start exploring the collection - download the first chapter of every title for free.

# Neglected culprit of nonlinear discharge characteristics in SF<sub>6</sub>: shielding effect induced by positive glow corona discharge

Zhicheng Wu<sup>1,4</sup> , Qiaogen Zhang<sup>1</sup> , Lisong Zhang<sup>1</sup> , Can Guo<sup>1,2</sup> ,  
Qiandong Du<sup>1,3</sup>  and Lei Pang<sup>1</sup> 

<sup>1</sup> State Key Laboratory of Electrical Insulation and Power Equipment, Xi'an Jiaotong University, Xi'an, People's Republic of China

<sup>2</sup> State Grid Shaanxi Electric Power Research Institute, Xi'an, People's Republic of China

<sup>3</sup> Nari Group Corporation (State Grid Electric Power Research Institute), Nanjing, People's Republic of China

E-mail: [z\\_c\\_wu@163.com](mailto:z_c_wu@163.com)

Received 31 March 2019, revised 5 June 2019

Accepted for publication 17 July 2019

Published 22 August 2019



## Abstract

The discharge characteristics of SF<sub>6</sub> dependent on gas pressure under extremely inhomogeneous electric fields are strongly nonlinear and must be carefully considered when optimizing gas-insulated equipment insulation design and defect detection. The main aim of this study was to determine the relationship between nonlinear breakdown characteristics and the pre-breakdown discharge mode transition. The breakdown model established by Niemeyer, as adapted under impulse voltage, was expanded. The images and the phase-resolved patterns of the pre-breakdown discharge as a function of gas pressure and applied voltage were analyzed to observe the relationship between them as per the spatial distribution of the spark paths. A universal model of the nonlinear breakdown phenomenon under steady-state voltage was established accordingly. Experimental results demonstrate the existence of a positive glow corona (PGC) discharge in the interval with the discontinuous breakdown voltage as well as significant interactions between the PGC discharge and leader discharge. The nonlinear characteristics can be attributed to the inception and quenching of the PGC discharge. The shielding effect induced by the PGC discharge is the neglected culprit of the strong nonlinear discharge characteristics under steady-state voltage. The nonmonotonic  $U$ - $p$  curve in electronegative gases was also assessed in an effort to build a theoretical basis for the manufacture and condition monitoring of the gas-insulated equipment.

Keywords: SF<sub>6</sub>, pre-breakdown discharge,  $U$ - $p$  characteristics, positive glow corona discharge, spark path spatial distribution

## 1. Introduction

Electronegative gases have a strong dielectric strength as they are able to attach to low-energy electrons [1–4]. SF<sub>6</sub> (or its mixture), a specific type of electronegative gas, has been applied in gas-insulated metal-enclosed switchgear (GIS) as an insulating medium [5, 6]. The discharge characteristics under different electric field distributions, especially the

breakdown characteristics, must be considered carefully to optimize any gas-insulated equipment insulation design [7–9]. The discharge characteristics dependent on gas pressure in extremely inhomogeneous electric fields are nonlinear; by contrast, they display an approximately linear trend in homogeneous electric fields [10–15]. The excellent dielectric strength of electronegative gases may be drastically reduced in an extremely inhomogeneous electric field. Although the occurrence of extremely inhomogeneous electric fields has been avoided in the compressed SF<sub>6</sub> structure by using

<sup>4</sup> Author to whom any correspondence should be addressed.

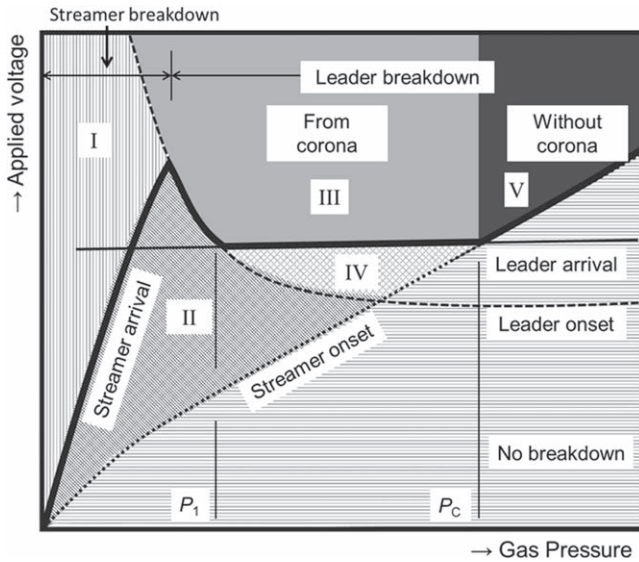


**Figure 1.** Contributed by Niemeyer (1983): a qualitative model of impulse breakdown in  $\text{SF}_6$  in inhomogeneous gaps separated by several limiting curves [18].

electric field optimization to avoid the occurrence of extremely uneven electric fields, the discharge characteristics under such electric field distributions also need to be considered due to particulate contamination.

The characteristics of breakdown voltage as they vary with gas pressure are expressed by the  $U$ - $p$  curve. This phenomenon was originally described by Sangasaad [16] and reviewed in detail by Farish *et al* [17]. Niemeyer *et al* [18] conducted groundbreaking research on nonlinear discharge characteristics. In 1983, they defined the nonlinear  $U$ - $p$  curve under impulse voltage by different pre-breakdown discharge modes separated by several limiting curves, for example, the breakdown mode transition from streamer to leader. Leader channels are considered more conductive than streamer channels, so the breakdown voltage drops once the leader channels appear (figure 1). In 2001, Boeck [19] referred to this phenomenon as ‘corona stabilization’ caused by antagonism between the development of the critical electric field and the migration of space charges. In 2005, Hayakawa [20] confirmed by experiment that the nonlinear variation of breakdown voltage in a  $\text{SF}_6/\text{N}_2$  mixture gas is closely related to the inception of leader discharge. The transition of a single discharge from streamer to leader was also observed in cases of varying pressure.

Previous research has investigated discharge characteristics under impulse voltage rather than steady-state voltage, which is the more common electric stress type in power systems. There is a marked difference in the  $U$ - $p$  curve under steady-state voltage versus transient voltage, so there is an urgent need to address the significant nonlinear discharge characteristics under steady-state voltage caused by the presence of space charges. In addition, previous research has focused on the streamer–leader transition, but ignores the transition of the discharge mode in the nonlinear region of the  $U$ - $p$  curve. In the present study, nonlinear characteristics were attributed to the inception and quenching of the positive

glow corona (PGC) discharge. The shielding effect induced by the PGC discharge is the neglected culprit of the strong nonlinear discharge characteristics under steady-state voltage.

The pre-breakdown discharge mode  $M$  can be determined by the applied voltage  $U$  and gas pressure  $p$ ; this correspondence can be expressed in a tuple  $M(U, p)$ . The main goal of the present study was to determine the relationship between the nonlinear breakdown characteristics and the transition of the discharge mode  $M(U, p)$ . The experimental setup is described in section 2. The images and phase-resolved patterns of the pre-breakdown discharge were used to identify the discharge modes. The spatial distribution of the breakdown spark paths reveals the effects of different pre-breakdown discharges on a given breakdown. The pre-breakdown discharge images and spark channel spatial distribution were investigated systematically in this study, as presented in section 3. Section 4 discusses the mechanism of the shielding effect induced by PGC discharge qualitatively, and presents the proposed universal model of the nonlinear breakdown phenomenon under a steady-state voltage. The nonmonotonic  $U$ - $p$  curve in electronegative gases was assessed in an effort to build a theoretical basis for the manufacture and condition monitoring of gas-insulated equipment.

## 2. Experimental setup

A schematic diagram of the experimental setup is shown in figure 2. We used a needle plane electrode system to form an extremely inhomogeneous electric field in  $\text{SF}_6$ . The needle electrode was fabricated in nickel as a hemispherical capped cylinder with a curvature radius of  $500\ \mu\text{m}$ . The plane electrode is made of stainless steel and well chamfered. The gap distance was set to precisely 10 mm. The electric field distribution of the electrode system was calculated by a boundary element method. The uniformity coefficient  $f$  is 15.2, so the electrode system produces a typical extremely inhomogeneous electric field. The electric field lines from the spherical tip of the point electrode towards the counter electrode are depicted at the bottom of figure 2. Furthermore, the normalized electric field along the rotational axis of symmetry (dashed-dotted line in the field line plot) is shown. The normalized electric field is obtained by setting the excitation voltage assigned to the needle electrode to 1 V. The previous research shows that the electrode chemical reactions during exposure to the  $\text{SF}_6$  corona discharge affect the discharge process by generating metal fluoride or metal sulfide on the electrode surface [21], so the exposure time in the corona discharge of each needle electrode was guaranteed to be less than 5 min.

The whole electrode system was placed in a sealed chamber to carry out our experiments across a wide gas pressure range. The experimental chamber was evacuated to vacuum (gas pressure  $<60\ \text{Pa}$ ), then filled with commercial  $\text{SF}_6$  (purity  $>99.997\%$ ) at gas pressure between 0.1 MPa and 0.5 MPa. The gas pressure was monitored with a Panasonic DP-102 digital pressure sensor.

Power frequency AC voltage (50 Hz) is the most common type of electric stress in electrical engineering, so we

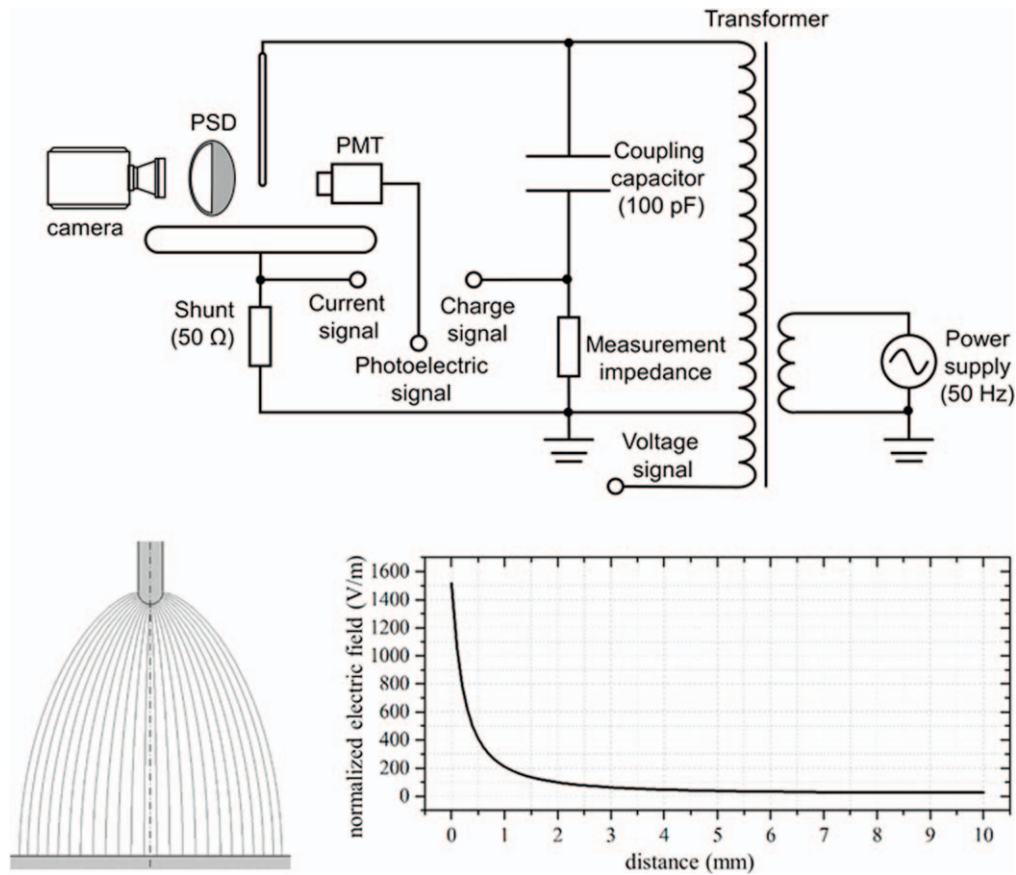


**Figure 2.** A schematic diagram of the experimental setup. The electric field lines and the normalized electric field along the rotational symmetry axis are shown at the bottom.

used it as the applied voltage for our experiment. The voltage was generated by a 400 kV/90 kVA gas-insulated test transformer and applied to the needle electrode via a damping resistor. A measuring winding with a voltage ratio of 1000:1 was used to measure the voltage waveform, and its combined standard uncertainty did not exceed 5% [22–24]. The amplitude of applied voltage is expressed here as a root mean square (RMS) unless otherwise specified. The applied voltage was increased at a constant rate (about  $1 \text{ kV s}^{-1}$ ) until breakdown occurred. We recorded the maximum applied voltage detected before breakdown as the breakdown voltage. The final value reported here is the average of three measurements. The needle electrode was changed after each breakdown to prevent any changes in electrode morphology due to spark erosion. Based on the IEC standard 60270-2015 [25], the apparent charge of the pre-breakdown discharge was coupled by a coupling capacitor and a measurement impedance. The amplitude of the discharge was calibrated by the charge calibrator Omicron CAL542.

As discussed above, we focused on the statistical patterns of the pre-breakdown discharge mode transition under different conditions rather than the transition of a single discharge process. High-speed framing or streak cameras are not used to observe a single discharge process. We used phase synchronization photography to prevent the discharges in different half cycles from occluding each other [26]. A phase synchronization device (PSD) was installed in front of a

camera and the central angle of the photography mask was set to  $180^\circ$  to take discharge images of positive or negative half cycles. We used a single lens reflex camera (Nikon D5) with an exposure time of 2.5 s and photosensitivity of ISO-102400.

Different spatial structures of space charges are formed by discharges of varying polarities and modes. This can affect the direction of the spark path at the moment of breakdown. We applied a three-dimensional (3D) reconstruction method by synthesizing two orthogonal discharge images [27, 28]. The deviation from the electrode axis can be expressed by the spatial launch angle.

### 3. Results

#### 3.1. Overview of $U$ - $p$ curve

The pressure dependence on the breakdown voltage can be expressed as a  $U$ - $p$  curve. The  $U$ - $p$  curve obtained in our experimental electrode system is shown in figure 3. It shows a strongly nonlinear trend: at a gas pressure below 0.175 MPa, the breakdown voltage increases approximately linearly at a rate of  $212 \text{ kV MPa}^{-1}$  and the breakdown voltage reaches a maximum at 0.175 MPa. The breakdown voltage at 0.2 MPa drops suddenly and is multivalued: 46 kV and 36 kV. At over 0.2 MPa, the breakdown voltage is insensitive to the gas pressure. At a gas pressure over



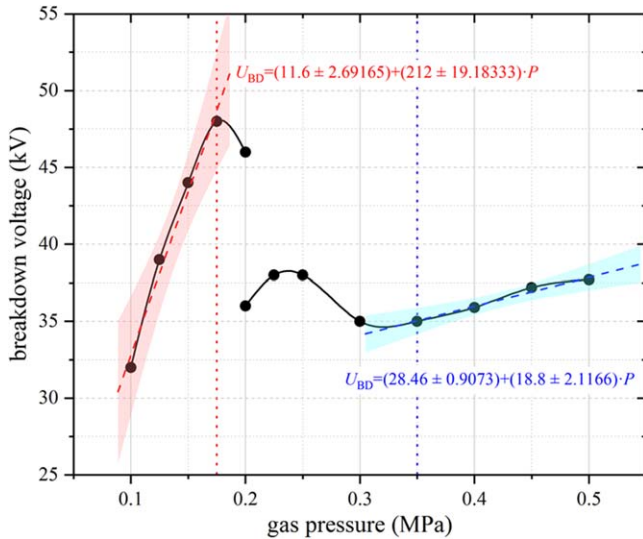


**Figure 3.** A typical  $U$ - $p$  curve: the breakdown voltage as a function of gas pressure. Confidence intervals (95%) are shaded.

0.35 MPa, the breakdown voltage increases linearly at a slower rate of about  $19 \text{ kV MPa}^{-1}$ .

The above  $U$ - $p$  curve cannot be fully explained by Niemeyer's model, as it does not include a steady corona. The  $U$ - $p$  curve under a steady-state voltage shows a more obvious nonlinear trend and is multivalued at a specific gas pressure. The breakdown characteristics are closely related to the pre-breakdown processes, which are more complex and influential than the case under an impulse voltage. Comprehensive, systematic assessments of the pre-breakdown discharge modes leading to breakdown are required to clarify the breakdown characteristics under a steady-state voltage. In this study, we used discharge images as a function of applied voltage and gas pressure to observe the discharge mode  $M(U, p)$ , and the spatial distribution of the spark path to discern the relationship between the breakdown and pre-breakdown discharge.

### 3.2. Images of pre-breakdown discharge

Each pre-breakdown discharge mode has a specific spatial appearance reflected in the discharge images. Here, we sought to distinguish different discharge modes to determine the tuple  $M(U, p)$  as a function of applied voltage and gas pressure.

The breakdown discharge occurs in the positive half-cycle regardless of variations in gas pressure. The breakdown voltage under positive DC voltage is lower than that under negative DC voltage [29]. We observed pre-breakdown discharges in the positive half-cycle and negative half-cycle by phase synchronization photography, as discussed above. The modes of the pre-breakdown discharges in the negative half-cycle appear to be Trichel or negative streamer discharges [30]. The appearance of pre-breakdown discharges in the negative half-cycle does not change significantly, that is, they do not correspond to a nonlinear process. Thus, the pre-breakdown discharges in the positive half-cycle are the cause of the nonlinear breakdown characteristics. We captured images of the

pre-breakdown discharges in the positive half-cycle at pressures between 0.1 MPa and 0.35 MPa accordingly.

The breakdown voltage and images as a function of applied voltage and gas pressure are shown in figure 4. The appearance of pre-breakdown discharge differs markedly across different gas pressures and applied voltages. The transition of pre-breakdown discharges as a function of applied voltage and gas pressure is discussed separately below.

At  $p = 0.1 \text{ MPa}$ , the luminous volume increases monotonically as the applied voltage increases. The shot is a time-averaged image, so the light-emitting area is very diffuse. The luminous volume surrounding the needle electrode consists of several streamer filaments, so the growing luminous volume corresponds to the growing streamer channel. According to Niemeyer's theory, the electric field strength inside the streamer channel is equal to the critical electric field in strongly electronegative gases [7, 31, 32]. The streamer channel stretches alongside the enhanced field ahead of the streamer tip. Once the channel reaches the grounded electrode, the highly conductive streamer channel transits to the spark channel leading to a breakdown discharge. This direct transition mode from streamer discharge to spark discharge is called 'streamer breakdown', as inherited from Niemeyer's model. The breakdown voltage estimation method we used in this study was first proposed by Ibrahim [33]. The breakdown criterion is considered to be the electric field threshold on the surface of the grounded electrode. Due to the existence of ion flow induced by corona discharge, the breakdown occurs if the normalized electric field threshold is greater than  $45 \text{ kV (mm} \cdot \text{MPa)}^{-1}$ . The shortcoming of this theory is that the polarity effect is not considered. The consensus is that the breakdown is directly caused by a direct transition from the streamer to the breakdown spark.

At  $p = 0.125 \text{ MPa}$ , the positive streamer discharge as a kind of dominant discharge mode under lower applied voltage is the same as that under a gas pressure of 0.1 MPa. When the applied voltage rises to 35 kV, clear and distinctive filaments appear below the needle electrode. When the applied voltage reaches 37 kV, these filaments appear below and on the side of the needle electrode. The filaments meet Niemeyer's definition of 'leader channels' [34]. The streamer channels are radially compressed as the gas pressure increases. The Joule heat caused by charge transfers through a thin channel leads to thermal expansion. The reduction of the gas density by the thermal expansion within the channel reduces the value of the electric gradient that is required to maintain its conductivity by ionization [35]. This strong ionized mode is confined to the thermally active channel of the leader channel—the length of the leader channel below the needle electrode is also much longer than those on the side of it.

At  $p = 0.15 \text{ MPa}$ , the appearance of the luminous volume differs significantly from that under a gas pressure of 0.125 MPa: it is a flat, diffuse shape surrounding the needle electrode. The volume increases as the applied voltage increases. Leader channels emerge until the applied voltage reaches 40 kV, at which point the channels seem to bypass the uniform luminous volume. The leader inception voltage at  $p = 0.15 \text{ MPa}$  in our experiment was higher than that at

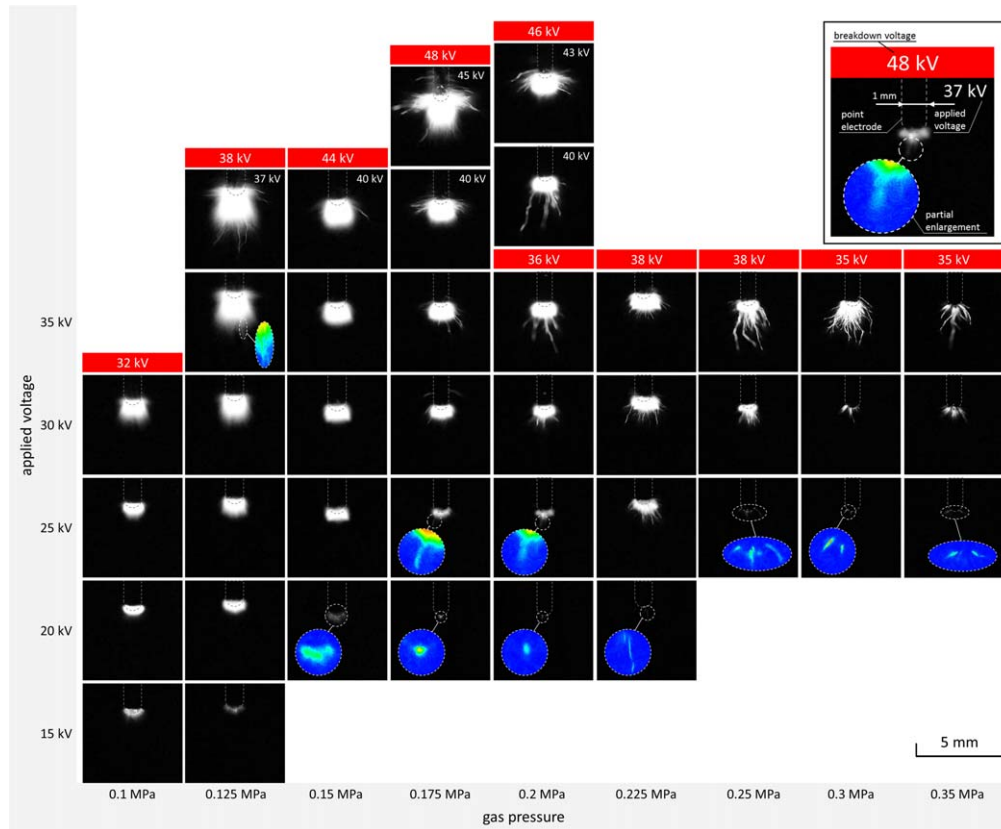


**Figure 4.** The breakdown voltage and images as a function of applied voltage and gas pressure. The breakdown voltage values are marked in red (two possible breakdown voltages at 0.2 MPa). Areas with low brightness contrast are processed with pseudo color and magnified.

$p = 0.125$  MPa, which is in conflict with the extant theory. In the model established by Niemeyer, the diameter of streamer channels is inversely proportional to gas pressure [36]. In other words, there is stronger thermal ionization and the leader inception voltage should decrease as the gas pressure increases. We infer that the behavior of the leader channels is affected by the uniform discharge surrounding the electrode. The phase-resolved patterns of pre-breakdown discharge confirm that this kind of uniform discharge is caused by the PGC discharge. The relationship between the apparent charge pulses and the voltage phase is shown in figure 5, where the pulses of the apparent charge signal near the positive peak disappear once the applied voltage reaches 30 kV. As the voltage increases, the sparse area of the discharge pulses at about  $90^\circ$  becomes wider. This indicates that pre-breakdown discharges at the positive peak have transited to pulseless discharges (or quasi-glow corona discharge). The same phenomenon can also be observed in corona discharges in the air [37]. The onset mechanism of positive glow discharge is discussed in detail in section 4. In summary, the presence of the PGC discharge significantly affects leader discharge behavior. There is a shielding effect induced by the positive glow discharge.

At  $p = 0.175$  MPa, the streamer discharge transited to a leader discharge when the applied voltage reached 25 kV.

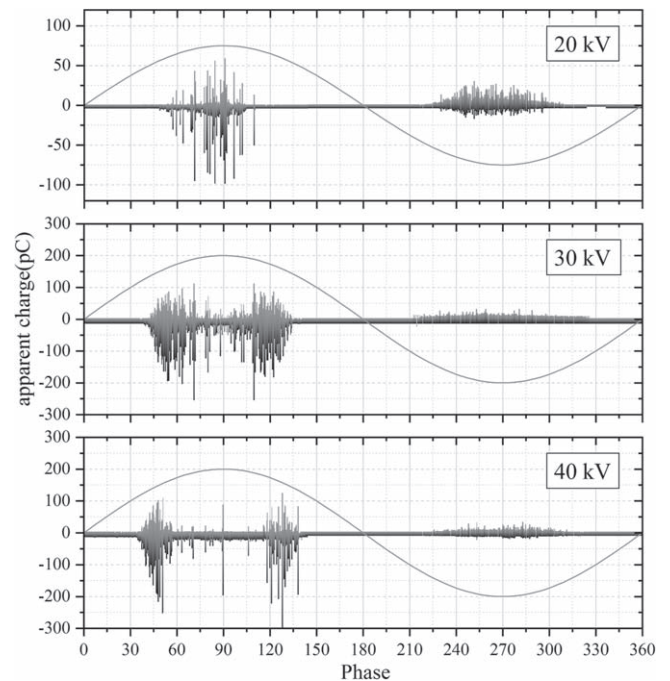


**Figure 5.** The phase dependence of the apparent charge signal under applied voltages of 20 kV, 30 kV, 40 kV under 0.15 MPa. The sparse area of discharge pulses near  $90^\circ$  widens as the voltage increases.

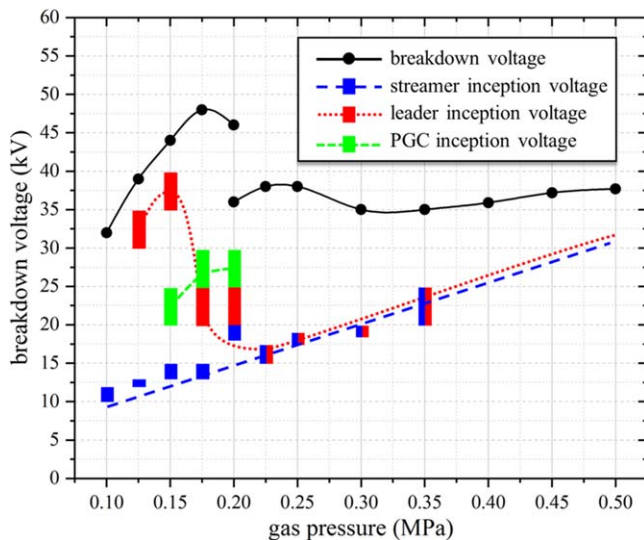


**Figure 6.**  $U$ - $p$  curve with limiting curves (onset voltage of streamer discharge, leader discharge, glow corona discharge). Side-by-side rectangles indicate the same onset voltage, i.e. simultaneous discharge processes.

Leader channels appeared along the axis of the needle electrode due to the absence of PGC discharge in this case, and moved gradually away from the axis as the applied voltage increased. Under the influence of the shielding effect of the PGC discharge, almost all the leader channels bypassed the volume directly below the needle electrode. As the applied voltage continued to rise, leader channels emerged below the needle electrode. The leader channels on the side of the electrode were longer than those below the electrode, which is different from the phenomenon we observed under a gas pressure of 0.125 MPa.

At  $p = 0.2$  MPa, we found that the discharge transition order was similar to that at  $p = 0.175$  MPa as the applied voltage increases. The leader channels below the electrode were much longer than those under 0.175 MPa. This phenomenon created multivalued breakdown voltages. When the applied voltage was 36 kV, the leader channels under the electrode were able to transit to the breakdown spark channel. Once the PGC incepted, these channels were shielded and became inclined. When the applied voltage was 46 kV, breakdown was caused by the leader channels on the side of the electrode. The multiplicity of the breakdown voltage appears to be caused by the leader channels below and on the side of the electrode, respectively. The essential cause of this behavior is the presence or absence of PGC.

At any gas pressure above 0.2 MPa, once the streamer channels formed, they transitioned to the leader channels. The length of the leader channels increased with the applied voltage, but was insensitive to gas pressure.

A set of limiting curves, including the inception voltage of the streamer discharge, leader discharge and glow corona discharge, are marked in the  $U$ - $p$  curve shown in figure 6. The onset criterion for the PGC discharge is based on a combination of the discharge images and the phase-resolved pattern. The nonlinear variations in breakdown voltage with

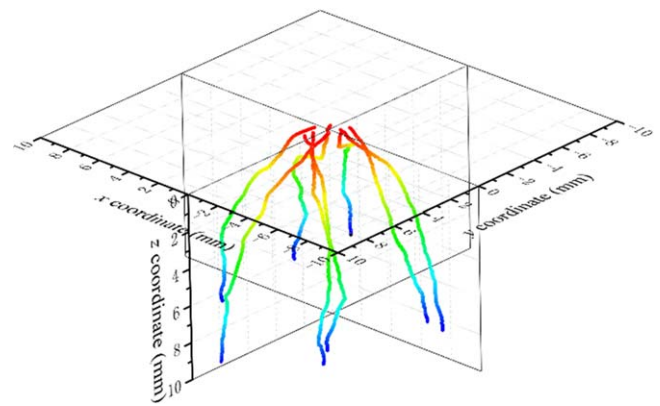


**Figure 7.** Three-dimensional spark paths under 0.175 MPa gas pressure. All spark paths deviate substantially from the electrode axis.

gas pressure are accompanied by a set of complex pre-breakdown discharge transition processes. Unlike the monotonical trend under an impulse voltage, the leader discharge inception voltage under a steady-state voltage does not monotonically decrease with increasing gas pressure, but rises and then falls. The shielding effect induced by the glow corona discharge is the cause of this. When the gas pressure exceeds the PGC quenching pressure, which in our case is 0.2 MPa, this shielding effect disappears.

Leader channel behavior appears to be significantly affected by the PGC discharge—whether the leader channels appear below or on the side of the needle electrode depends on the presence of the PGC discharge, and the transition from streamer discharge to leader discharge can only occur outside the PGC discharge volume. This volume increases as the applied voltage increases, and decreases as the gas pressure increases. The PGC discharge disappears when the gas pressure is higher than 0.2 MPa, and the transition no longer falls under the shielding effect. Thus, the shielding effect induced by the PGC discharge is the neglected culprit of the nonlinear discharge characteristics in  $\text{SF}_6$ .

### 3.3. Spark path spatial distribution

The spark path leading to breakdown may be sensitive to the transient electric field or space charge; thus the spatial distribution of the spark path reflects space charge behavior. In this study, we investigated the spark path spatial distributions via 3D reconstruction. The 3D spark paths under a gas pressure of 0.175 MPa are shown in figure 7; all paths greatly deviate from the electrode axis due to the presence of the PGC discharge volume below the electrode. The spatial launching angle can be defined as the acute angle between the spark path and the electrode axis and can be calculated by two orthogonal discharge images. A spatial launching angle close to  $90^\circ$  indicates that the spark path greatly deviates from the electrode axis.

We measured the spatial launching angles of spark paths under pressures between 0.1 MPa and 0.5 MPa, as shown in figure 8. Due to the large dispersion of these data, a scatter



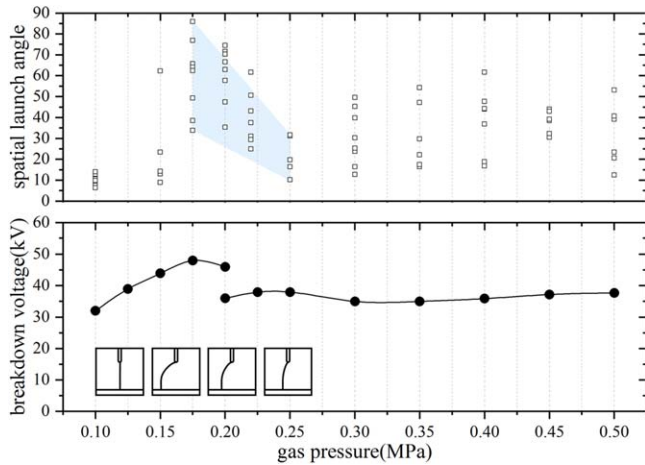


**Figure 8.** The spatial launch angle as a function of gas pressure. Larger angles indicate a greater deviation from the electrode axis. The shaded area marks a decreasing angle at intervals with discontinuous breakdown voltage under increasing gas pressure.

diagram was used to express the relationship between the gas pressure and spatial launching angle rather than statistical parameters (e.g. averages). Independent experiments in each specific condition were repeated at least five times. We found that under a gas pressure below 0.175 MPa, the spatial launch angle values and their deviations were small—that is, the spark paths were close to the electrode axis. Under 0.175 MPa, both the spatial launch angle and the breakdown voltage reached their respective maximum and there was a wide deviation in the spatial launch angle. A breakdown with a launch angle of about  $90^\circ$  emerged in the experiments. The angle decreased as the gas pressure increased, which is marked with a shadow in figure 7. The pressure dependence on the spatial launch angle was no longer evident when the gas pressure increased to 0.3 MPa.

The relationship between the spatial launch angle and gas pressure can be observed in pre-breakdown discharge images. When the gas pressure falls into the streamer breakdown interval, the breakdown spark path transits from the streamer channel to the spark channel which is perpendicular to the plane electrode; thus the value and the deviation of the spatial launch angle are small. As the gas pressure increases and the glow corona discharge appears, the leader channels must bypass the volume of the glow corona discharge; they transit to breakdown spark paths thus creating a much larger spatial launch angle. In some extreme cases, the spark paths can be perpendicular to the needle electrode. As the gas pressure continues to increase, the volume of the glow corona discharge decreases and the shielding effect is weakened; thus the angle decreases. If the gas pressure is above the PGC quenching pressure, the spatial distributions of the spark paths are determined by the transition from random leader channel to spark channel; thus the deviation is large and has no relation to the gas pressure.

In summary, the gas pressure dependence on the spatial launch angle confirms the decisive influence of nonlinear discharge characteristics caused by the PGC discharge.

## 4. Discussion

We investigated the pre-breakdown discharge appearance and spark path distributions to prove that PGC discharge is the fundamental cause of nonlinear discharge characteristics in  $\text{SF}_6$ . We also qualitatively analyzed the shielding effect induced by this discharge mode to build a universal model of nonlinear characteristics of  $\text{SF}_6$  breakdown discharge, which is essentially an extension of Niemeyer's model.

According to the classification of corona discharge in atmospheric air by Chang [38], discharges in positive polarity start with a burst pulse corona and proceed to a streamer corona, glow corona and spark discharge as the applied voltage increases. The discharge in  $\text{SF}_6$  is quite similar in atmospheric air. Hermstein [39] first proposed the now widely accepted theory of PGC discharge inception, where photoionization induced by frequent recombination between negative charges gathers near the needle electrode and positive charges are the positive feedback condition that causes the discharges. In 1999, Akishev [40] indicated that the soft X-radiation induced by *bremstrahlung* provides fast positive feedback for electron avalanches through the ionization region of the corona. However, Akishev's theory was later refuted by Aints [41] who reconfirmed that positive feedback is the photoionizing radiation emitted by gas molecules or atoms. In summary, the mechanism of PGC is still unclear—but it does indeed appear more easily in electronegative gas than in electropositive gas. In electronegative gas, an amount of negative ions accumulates in the vicinity of the positive electrode with a small curvature radius, and a relatively homogeneous electric field forms between the negative ions and the positive electrode. The breakdown discharge occurs in this region and this thin layer of ionized gas forms a stable PGC discharge.

The characteristic light emission pattern of the PGC discharge is very similar to the classic low-pressure glow discharge described in detail throughout the literature [42]. The space charge distribution near the needle electrode of the PGC discharge is considered to be similar to that near the anode of glow discharge in a uniform electric field [43, 44]. Thus, the theory of glow discharge can be used to qualitatively explain the shielding effect induced by PGC discharge. There is a thin anodic sheath close to the positive electrode formed by negative ions and a positive column region with a large volume beyond this sheath, which comprises the majority of the positive glow discharge [45, 46]. The positive column region is quasi-neutral ionized and the internal electric field strength is only sufficient to merely sustain ionization. When the region below the electrode is shielded by the positive column region and the electric field strength is reduced, the streamer channels cannot transit to leader channels due to the insufficient electric field strength. Streamer channels on the side of the needle electrode are not affected by this shielding, so they more easily transit to the leader channels as the applied voltage increases and form a spark path leading to breakdown.

The relationship between the PGC discharge and the spatial distribution of the spark paths can be determined by



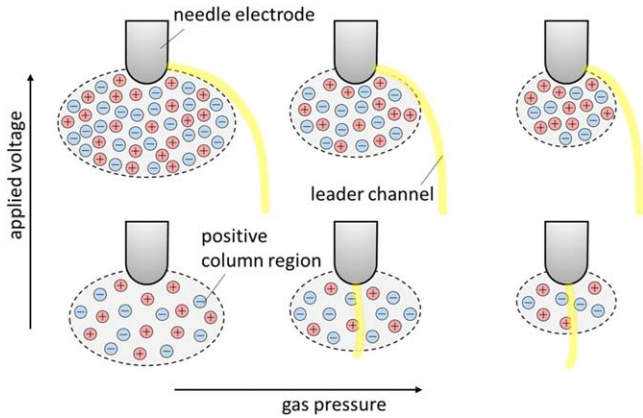


**Figure 9.** The spark path affected by the PGC discharge shielding effect. The PGC discharge volume varies with applied voltage, and the gas pressure determines the spark path spatial distribution.

analyzing the behaviors of the positive glow discharge, as shown in figure 9. The volume of PGC discharge increases as the applied voltage increases and is compressed by an increase in gas pressure. A larger glow corona discharge volume indicates a better shielding effect for the leader channel, which prevents it from appearing in the volume of the PGC discharge. The length of the leader channel also increases as the applied voltage increases. The competition between the increasing rate of the PGC volume and the leader channel length is the primary cause of nonlinear discharge characteristics. When the former is larger than the latter, leader channels are more likely to appear outside the positive column region. The spatial distribution of spark paths forms a series of straight lines along the electrode axis. In contrast, when the former is smaller than the latter, the electric field inside this region is too high and the leader channels can penetrate the region. The spatial distribution of spark paths forms a series of inclined lines with a large spatial launch angle.

In conducting this study, we also sought to determine why the breakdown voltage drops suddenly once the gas pressure exceeds a specific value, or, in other words, why the shielding effect of the PGC may suddenly disappear. The volume of the PGC decreases continuously as the gas pressure increases, thus the breakdown voltage should have decreased continuously in our experiment (section 3.2). We found the opposite to be true: the PGC disappeared suddenly once the gas pressure exceeded a specific value. As shown in figure 3, we measured the breakdown voltage with a gas pressure of 0.225 MPa as 36 kV by increasing the applied voltage at a constant rate. We call increasing the applied voltage with a fixed gas pressure ‘approach I’. In ‘approach II’, we increased the applied voltage to 42 kV with a gas pressure of 0.175 MPa, then slowly filled the gas to 0.225 MPa.

The results of applying approaches I and II are shown in figure 10. The discharge image of the ‘withstand’ group shows the existence of a PGC discharge, and the discharge image of the ‘breakdown’ group shows an elongated leader channel. We found that the pre-breakdown discharge was not

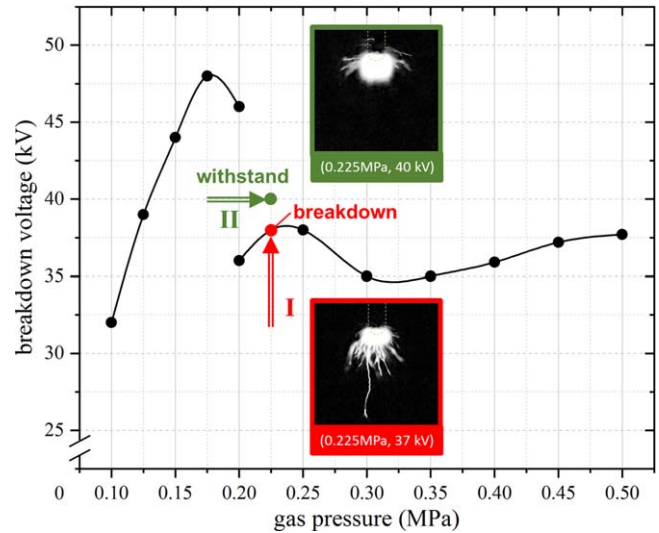


**Figure 10.** Breakdown or withstanding caused by approach I (increase applied voltage with fixed gas pressure) and approach II (increased gas pressure with fixed applied voltage). The subfigures show the discharge image captured via approach I (0.225 MPa, 37 kV) and approach II (0.225 MPa, 40 kV), respectively.

transited to the breakdown discharge by approach II, influenced by the shielding effect induced by the PGC discharge. Two completely different experimental results were obtained under completely identical experimental conditions, which forms a paradox. Our only explanation is that the electric field was influenced by the different distributions of space charges formed by the different approaches. We assumed that the PGC would be able to sustain at a higher gas pressure, but the transition from streamer discharge to PGC discharge was no longer satisfied during this experiment. That is, the PGC did not disappear as the gas pressure increased slightly if the discharge had been onset, thus the shielding effect remained.

The universal model we built to explain the nonlinear breakdown phenomenon under steady-state voltage is shown in figure 11. The model was drawn according to Niemeyer’s model and supplemented for cases under steady-state voltage. The horizontal axis (gas pressure) was divided into six parts at five gas pressure values from  $P_1$  to  $P_5$ . The different filling forms in the figure represent different pre-breakdown discharge modes.

- $P < P_1$ : Streamer discharge is the exclusive discharge mode. The streamer channel transits to the breakdown spark path when a breakdown occurs. The channel develops along with the electric field direction, so the breakdown spark path is perpendicular to the plane electrode. The streamer arrival limit can be calculated by considering the electric field threshold on the surface of the grounded electrode.
- $P_1 < P < P_2$ : Streamer discharge, as the dominant pre-breakdown discharge, transits to the leader discharge at higher applied voltages. All leader channels are located below the needle electrode. The breakdown voltage starts to deviate from the streamer arrival limit due to the higher conductivity of the leader channel. The breakdown is

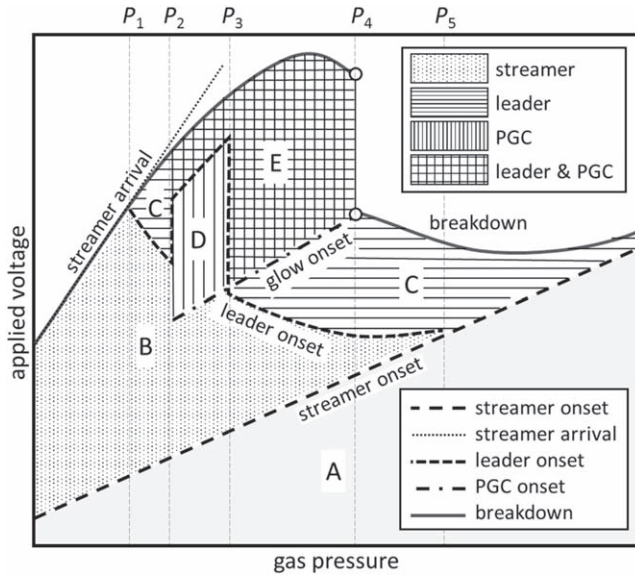


**Figure 11.** The universal model of the nonlinear breakdown phenomenon under a steady-state voltage.

determined by the leader discharge, thus, a large angle forms between the spark path and electrode.

- $P_2 < P < P_3$ : In order, the pre-breakdown discharge modes are the streamer discharge, glow corona discharge and leader discharge. The transition from streamer discharge to leader discharge below the electrode is suppressed by the shielding effect of the glow corona discharge, thus the leader inception voltage increases. The streamer channels on the side of the electrode transit to the leader channels under a higher applied voltage. The leader channels bypass the glow corona discharge volume. The breakdown spark is transited from these leader channels; the spark path and the electrode axis form a large angle.
- $P_3 < P < P_4$ : The shielding effect induced by the glow corona discharge is weakened. The streamer channels below the electrode transit to leader channels. These leader channels may cause breakdown with straight spark paths. As the applied voltage increases, the leader channels are suppressed upon glow corona discharge inception. When the streamer channels on the side of the electrode meet the transition condition from streamer channels to leader channels, inclined channels are formed. The spatial launch angle of the spark path is smaller than that in the previous case due to the weaker shielding effect. The multiplicity of the breakdown voltage is caused by the leader channels below and on the side of the electrode, respectively, corresponding to the presence or absence of PGC. Lower and higher breakdown voltages are thus related to straight and inclined spark paths, respectively.
- $P_4 < P < P_5$ : The transition from streamer discharge to leader discharge cannot happen in this pressure region. Once the streamer discharge incepts, the streamer channels transit to the leader discharge. To this effect, the breakdown spark is dependent on the length of the

leader channel. The random positions of leader channels lead to large deviations in the spark path launch angles. It is worth mentioning that the length of the leader channels in this interval may be related to the circuit impedance. At present, the reduction of gas density may occur not only within the expanding channel but also in the space ahead of the leader tip; thus the leader step generation model can be described by the gas dynamics of a spherical shock wave [35]

- $P > P_5$ : The streamer channels transit to leader channels and arrive at the grounded electrode immediately. Thus, the breakdown voltage is determined by the streamer inception limiting curve. The onset voltage for positive streamer discharge can be estimated via the method described by Abdel-Salam [47].

## 5. Conclusions

The breakdown characteristics in  $\text{SF}_6$  with a varying gas pressure and in an extremely homogeneous electric field under a steady-state voltage show much stronger nonlinear trends than those under impulse voltage. To investigate this phenomenon, we expanded the breakdown model established by Niemeyer to adapt it to the steady-state voltage, then analyzed photographic images and phase-resolved patterns of pre-breakdown discharge as a function of gas pressure and applied voltage. We determined the relationship between the pre-breakdown discharge processes and breakdown discharge by analyzing the spatial distribution of the spark paths. Our results can be summarized as follows.

- (1) According to the discharge images and the phase-resolved pattern, PGC discharge occurs in the interval of the discontinuous breakdown voltage. At a certain pressure interval, it is a flat shape surrounding the needle electrode. The sparse area of the pre-breakdown discharge pulses at about  $90^\circ$  become wider as the applied voltage increases. These phenomena confirm the existence of a PGC discharge, which plays an important role in the behavior of leader channels: whether the leader channels appear below or on the side of the needle electrode depends on the presence of the PGC discharge. In general, leader channels do not appear in the volume of the PGC discharge. Affected by the presence of the PGC, the transition from streamer to leader becomes difficult and the leader discharge onset voltage increases. The leader channels emerge under higher applied voltages and bypass the volume of the PGC discharge.
- (2) We explored the relationship between the pre-breakdown discharge processes and breakdown discharge by analyzing the spatial distributions of spark paths. The spatial launch angle, as a function of gas pressure, increases in the presence of PGC discharge. The volume of PGC discharge is compressed by increasing the gas pressure, so the spatial launch angle decreases.

The spatial launch angle becomes random if the PGC discharge quenches.

- (3) The gas pressure can be divided into six parts according to the transition order from different pre-breakdown discharge processes. This constitutes a universal model of the nonlinear breakdown phenomenon under a steady-state voltage. In this model, the role of the unique discharge mode (PGC discharge) is emphasized. The shielding effect induced by the PGC discharge is the neglected culprit of nonlinear discharge characteristics in SF<sub>6</sub>.

This study was limited to a specific electrode system, and it is not fully possible to generalize qualitative models to quantitative models. A similar study may be carried out in the future on other electric field distributions. Research is also yet needed to determine several other important parameters, for example, the onset voltage or quenching pressure of PGC discharges. The plasma parameter in the volume of the PGC discharge also represents an intriguing yet unanswered question which may merit further research. For instance, a comparison of the electron temperature and gas temperature could provide strong evidence of PGC discharges.

## ORCID iDs

Zhicheng Wu  <https://orcid.org/0000-0003-3498-7520>  
 Qiaogen Zhang  <https://orcid.org/0000-0002-3722-8733>  
 Lisong Zhang  <https://orcid.org/0000-0002-5521-2786>  
 Can Guo  <https://orcid.org/0000-0002-5046-5338>  
 Qiandong Du  <https://orcid.org/0000-0003-1390-9945>  
 Lei Pang  <https://orcid.org/0000-0002-1168-8176>

## References

- [1] Christophorou L G and Olthoff J K 2000 *J. Phys. Chem. Ref. Data* **29** 267
- [2] Phelps A V and Van Brunt R J 1988 *J. Appl. Phys.* **64** 4369
- [3] Osmokrovic P 1989 *IEEE Trans. Power Del.* **4** 2095
- [4] Osmokrovic P 2007 *Plasma Source Sci. Technol.* **16** 643
- [5] Osmokrovic P et al 2012 *IEEE Trans. Dielectr. Electr. Insul.* **19** 677
- [6] Koch H et al 2018 *IEEE Trans. Dielectr. Electr. Insul.* **25** 1448
- [7] Seeger M and Clemen M 2013 *J. Phys. D: Appl. Phys.* **47** 25202
- [8] Malik N H and Qureshi A H 1979 *IEEE Trans. Electr. Insul.* **1** 1
- [9] Wu Z et al 2018 *IEEE Trans. Dielectr. Electr. Insul.* **25** 1454
- [10] Hazel R and Kuffel E 1976 *IEEE Trans. Power App. Syst.* **95** 178
- [11] Wiegart N et al 1988 *IEEE Trans. Power Del.* **3** 923
- [12] Wiegart N et al 1988 *IEEE Trans. Power Del.* **3** 931
- [13] Wiegart N et al 1988 *IEEE Trans. Power Del.* **3** 939
- [14] Seeger M, Niemeyer L and Bujotzek M 2008 *J. Phys. D: Appl. Phys.* **41** 185204
- [15] Wu Z et al 2017 *Proc. of the IEEE Electrical Insulation Conf. (EIC 2017) (Baltimore, Maryland, USA, June 11–14)* p 66
- [16] Sangkasaad S 1975 *Proc. of 2nd Int. Symp. on HV Technology (Zurich, Switzerland, September 9–13)* p 379
- [17] Haddad A and Warne D 2004 *Advances in High Voltage Engineering* (London: Institution of Electrical Engineers) p 58
- [18] Pinnekamp F and Niemeyer L 1983 *J. Phys. D: Appl. Phys.* **16** 1293
- [19] Hinterholzer T and Boeck W 2000 *Annual Report of the Conf. on Electrical Insulation and Dielectric Phenomena (CEIDP 2000) (Victoria, British Columbia, Canada, October 15–18)* p 413
- [20] Hayakawa N et al 2006 *IEEE Trans. Dielectr. Electr. Insul.* **13** 842
- [21] Wu Z et al 2018 *Phys. Plasmas* **25** 72104
- [22] Jusic A et al 2018 *Nucl. Technol. Radiat. Protection* **33** 2018 260
- [23] Perazic L et al 2018 *Nucl. Technol. Radiat. Protection* **33** 2018 268
- [24] Arbutina D et al 2017 *Nucl. Technol. Radiat. Protection* **32** 2017 250
- [25] International Electrotechnical Commission 2015 *High-voltage test techniques - Partial discharge measurements IEC 60270* International Electrotechnical Commission
- [26] Wu Z et al 2018 *Rev. Sci. Instrum.* **89** 56107
- [27] Nijdam S et al 2008 *Appl. Phys. Lett.* **92** 101502
- [28] Wu Z et al 2018 *Proc. of the IEEE Int. Power Modulator and High Voltage Conf. (IPMHVC 2018) (Jackson, Wyoming, USA, June 3–7)*
- [29] Malik N H et al 1983 *IEEE Trans. Electr. Insul.* **6** 629
- [30] Negara Y et al 2007 *IEEE Trans. Dielectr. Electr. Insul.* **14** 91
- [31] Seeger M, Niemeyer L and Bujotzek M 2009 *J. Phys. D: Appl. Phys.* **42** 185205
- [32] Korasli C and Farish O 1982 *Gaseous Dielectrics III* (New York: Pergamon) p 77
- [33] Ibrahim O E 1985 *Electr. Power Syst. Res.* **8** 127
- [34] Niemeyer L, Ullrich L and Wiegart N 1989 *IEEE Trans. Electr. Insul.* **24** 309
- [35] Waters R 2019 *J. Phys. D: Appl. Phys.* **52** 025203
- [36] Bujotzek M et al 2015 *J. Phys. D: Appl. Phys.* **48** 245201
- [37] Wu Z 2019 *IEEE Trans. Dielectr. Electr. Insul.* **26** 898
- [38] Chang J S, Lawless P A and Yamamoto T 1991 *IEEE Trans. Plasma Sci.* **19** 1152
- [39] Hermstein W 1960 *Arch. Elektrotechnik* **45** 279
- [40] Akishev Y S et al 1999 *J. Phys. D: Appl. Phys.* **32** 2399
- [41] Aints M et al 2001 *J. Phys. D: Appl. Phys.* **34** 905
- [42] Raizer Y P 1991 *Gas Discharge Physics* (Berlin: Springer)
- [43] Morrow R 1997 *J. Phys. D: Appl. Phys.* **30** 3099
- [44] Bruggeman P et al 2008 *J. Phys. D: Appl. Phys.* **41** 215201
- [45] Nijdam S et al 2012 *Plasma Chemistry and Catalysis in Gases and Liquids* (New York: Wiley-VCH) p 40
- [46] Staack D et al 2005 *Plasma Sources Sci. Technol.* **14** 700
- [47] Abdel-Salam M and Stanek E K 1988 *IEEE Trans. Ind. Appl.* **24** 1025